A Phase Detection Method using Power Handling Capability in Resonant Converters

Ahmad, Faheem; Jørgensen, Asger Bjørn; Munk-Nielsen, Stig; Beczkowski, Szymon

Published in:
2023 25th European Conference on Power Electronics and Applications, EPE 2023 ECCE Europe

DOI (link to publication from Publisher):
10.23919/EPE23ECCEEurope58414.2023.10264445

Publication date:
2023

Document Version
Accepted author manuscript, peer reviewed version

A Phase Detection Method using Power Handling Capability in Resonant Converters

Faheem Ahmad, Asger Bjørn Jørgensen, Stig Munk-Nielsen, Szymon Michal Beczkowski
AAU ENERGY, AALBORG UNIVERSITY
Pontoppidanstraede 101
9220 Aalborg, Denmark
E-Mail: faah, abj, smn, sbe@energy.aau.dk

URL: https://www.energy.aau.dk

***Index Terms*—Control strategy, converter circuit, emerging topology, high frequency power converter, resonant converter.**

***Abstract*—In resonant converter, controlling phase angle is important as insufficient phase can lead to semiconductor devices to enter complete or partial hard-switching conditions. This is exceptionally challenging when operating at multi-MHz switching frequency. This paper proposes a concept of calculating phase angle from resonant topology inherent property of power handling capability. A Class-PN resonant converter topology is operated with a series-parallel compensated load at 6.76 MHz. The phase angle is measured using experimental waveforms and compared with calculated values by proposed methodology of using the power handling capability. The proposed methodology calculates phase angle with an error of 3.2-6.6° compared to measurement when the input DC voltage is varied from 180-300 V.**

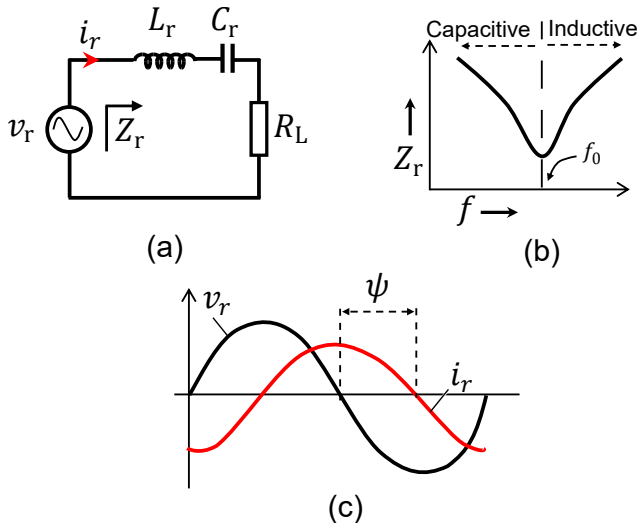

Fig. 1. Voltage source resonant converter connected to series resonant load (a) schematic, (b) impedance curve, and (c) waveform.

I. Introduction

Modern wide bandgap (WBG) semiconductor technology such as silicon carbide (SiC) and gallium nitride (GaN) devices have an order of magnitude lower junction capacitance than silicon counterparts. This leads to exceptional switching capability with small switching losses. The obvious progression to take advantage of low switching losses was to increase the switching frequency and increase power density of the converter [1]. However, in order to increase the switching frequency even further to MHz region requires resonant converter topologies to achieve soft-switching operation. To maintain soft-switching in resonant converter, sufficient reactive energy is required to charge-discharge the output capacitance (C_{OSS}) of the semiconductor device [2]. Fig. 1(a) shows schematic of a voltage source (v_{r}) connected to series resonant load. The voltage source (v_{r}) represents a voltage source resonant converter. Since the resonant converter is a voltage source type, the impedance seen by the resonant converter has to be inductive represented by Z_{r} here. Fig. 1(b) plots the impedance (Z_{r}) versus frequency curve for the series resonant load comprised of inductor (L_{r}) and capacitor (C_{r}). As shown, the impedance is minimum at the load natural frequency ($f_0 = 1/2\pi\sqrt{L_{\mathrm{r}}C_{\mathrm{r}}}$). The right side of natural frequency (f_0) represents inductive load region. The operating frequency of voltage source resonant converter (f_{SW}) has to be in this region for soft-switching operation. Fig. 1(c) shows the voltage and current waveforms for the resonant converter. The phase difference (ψ) is such that the load current (i_{r}) lags the converter voltage (v_{r}), representing operation in inductive region of load.

High frequency resonant converters are used in com-

mercial applications such as wireless power transfer (WPT), induction heating and medical applications [2]–[4]. In practical applications the load dynamics does not remain same and varies based on several factors, such as the distance or orientation between transmission and receiving coils in WPT or the temperature of work material in induction heating [5], [6]. Thus the natural frequency of the load (f_0) varies. To ensure that the resonant converter operating frequency (f_{SW}) remains in the inductive region and sufficient phase angle is maintained to achieve soft-switching. A closed-loop system is developed based either on zero cross detection (ZCD) or phase locked loop (PLL) controller. Several industrial application have utilized PLL based closed-loop control on resonant converter topology like full-bridge series LLC or Class-E with LCC series-load [7]–[9]. ZCD mechanism is another methodology, used frequently in converters operating in boundary conduction mode [10], [11]. ZCD in both these works is used for controlling the gate signal of synchronous rectification such that the devices can achieve soft-switching and improve system efficiency. Similarly in LLC resonant DC-DC converters for high power, high current applications, ZCD is used to find switching instant of synchronous rectification in soft-switching operation [12], [13]. The work in [12] is based on current sensing technique using current transformer (CT), while [13] is based on voltage detection. However both these ZCD technique have been criticized. For example current sensing transformer (CT) is bulky and leads to large power loss, while voltage sensing solution are prone to noise due to circuit parasitic inductance. Therefore alternative approaches have been proposed in literature to develop closed-loop control based on the understanding of converter topology [14], [15]. These alternative approaches may not be universally applicable to all converter topologies however they have better performance. In this paper, a phase detection method for a high frequency resonant converter is presented. The presented methodology also utilizes an inherent property of resonant converter called power handling capability and requires only the DC input current and peak value of output AC current of the converter to calculate phase. A four-switch resonant topology called Class-PN is used as a voltage source resonant converter [16]. Phase angle calculation on experimental results of a series-parallel resonant load have been presented.

Section II explains the relationship between the phase angle and the input, output current of the Class-PN resonant converter. Section III presents experimental results of Class-PN at four operating points and measures the phase angle using experimental waveforms and compares it to calculated values. Finally, section IV takes into account the compensation for current measurement probe and provides adjusted values for the measured phase angle.

II. Phase Calculation using Power Handling Capability of Class-PN

The power handling capability or normalized power handling capability has been used as a figure-of-merit (FOM) to evaluate a resonant topology [17]. It is defined as the ratio of maximum voltage subjected to semiconductor switch drain-source (V_{SM}) to the DC link voltage (V_{DC}), multiplied by the ratio of peak current through the switch (I_{SM}) and the DC current (I_{DC}). The power handling capability (c_p) is defined as (1),

$$c_{\text{p}} = \frac{V_{\text{DC}}}{V_{\text{SM}}} \cdot \frac{I_{\text{DC}}}{I_{\text{SM}}} \tag{1}$$

Lower value of power handling capability means worse device utilization. In [16], it is shown that Class-PN has a power handling capability of 0.636 which is more than 6x higher than other single-switch topology like Class-E. Higher power handling capability in Class-PN is due to V_{SM} being equal to V_{DC} as shown in Fig. 2(b). Power handling capability for Class-PN can be derived from its operation behavior. Fig. 2(a) shows the schematic of Class-PN connected to a series resonant RLC load.

As the output voltage (v_{r}) is a dual-pole DC voltage application (Positive and Negative) on the resonant load. The ouput voltage and current waveforms for Class-PN shown in Fig. 2(b) is defined as (2).

$$\begin{aligned} v_{\text{r}} &= \begin{cases} -V_{\text{DC}} & \in \quad (0, \pi] \\ V_{\text{DC}} & \in \quad (\pi, 2\pi] \end{cases} \\ i_{\text{r}} &= I_{\text{SM}} sin(\omega t - \psi) \qquad \in \quad (0, 2\pi] \end{aligned} \tag{2}$$

In (2) the output voltage transition have been neglected for simplifications. It can be seen that the current (i_{r}) through the resonant RLC load has a phase delay of ψ, because the load is tuned to be inductive at the operation frequency (f_{SW}). Based on the switching scheme, the current through the four switches is expressed as (3),

$$\begin{aligned} i_{\text{S1}} = i_{\text{S4}} &= \begin{cases} 0 & \in \quad (0, \pi] \\ I_{\text{SM}} sin(\omega t - \psi) & \in \quad (\pi, 2\pi] \end{cases} \\ i_{\text{S2}} = i_{\text{S3}} &= \begin{cases} -I_{\text{SM}} sin(\omega t - \psi) & \in \quad (0, \pi] \\ 0 & \in \quad (\pi, 2\pi] \end{cases} \end{aligned} \tag{3}$$

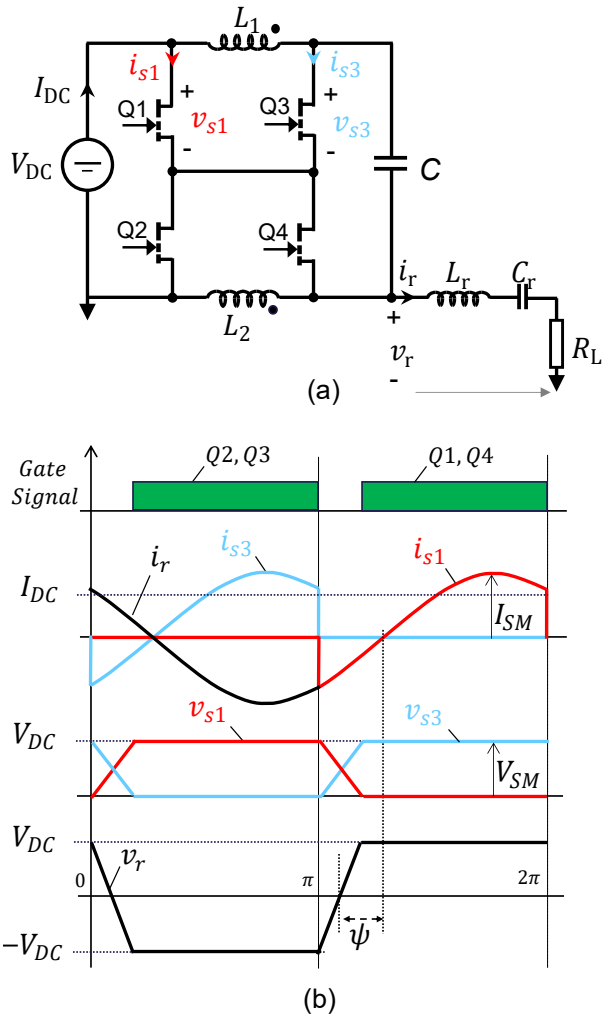

Fig. 2. Class-PN topology with a resonant load (a) schematic, and (b) voltage and current through switches and load current in a single period.

By combining the current through the devices, DC input current from the DC link can be presented as (4),

$$I_{\mathrm{DC}} = \frac{1}{\pi}\int_0^{\pi} I_{\mathrm{SM}} sin(\omega t - \psi)\ \mathrm{d}(\omega t) = \frac{2I_{\mathrm{SM}} cos(\psi)}{\pi} \quad (4)$$

The power handling capability of 0.636 in Class-PN is a theoretical limit and achieved when the converter is operating at load natural frequency, i.e., $f_{\mathrm{SW}} = f_0$ and the phase angle (ψ) is 0, i.e., $cos\psi \rightarrow 1$ in (4). However, as Class-PN is a voltage source type resonant converter topology that requires reactive energy from the load to achieve soft-switching as discussed in section I. Thus the converter is operated in the inductive region of the load. Therefore, (4) can be rewritten as (5),

$$\psi = cos^{-1}\left(\frac{I_{\mathrm{DC}}}{I_{\mathrm{SM}} \cdot \frac{2}{\pi}}\right) \quad (5)$$

Thus in Class-PN by only measuring the peak value of output resonant current (I_{SM}) and converter input DC current (I_{DC}), one can calculate the phase angle of load (ψ).

III. Experimental Results of Class-PN

To validate the methodology, phase angle between the Class-PN output voltage and current waveform are measured and compared to the value calculated by (5) at different operating points. Class-PN is operated with a series-parallel compensated resonant load. Fig. 3(a) shows the compensated resonant load network. The primary and secondary side are coupled via a core-less high frequency transformer. k is the coupling co-efficient between the winding. Because of the core-less design the winding are weakly coupled ($k < 1$). Therefore, the primary side winding (L_{P}) is series compensated by capacitor (C_{P}), while the secondary winding is compensated by capacitor (C_{S}) in parallel to winding (L_{S}). R_{P}, R_{S} represent the winding equivalent series resistance (ESR) on primary and secondary side respectively.

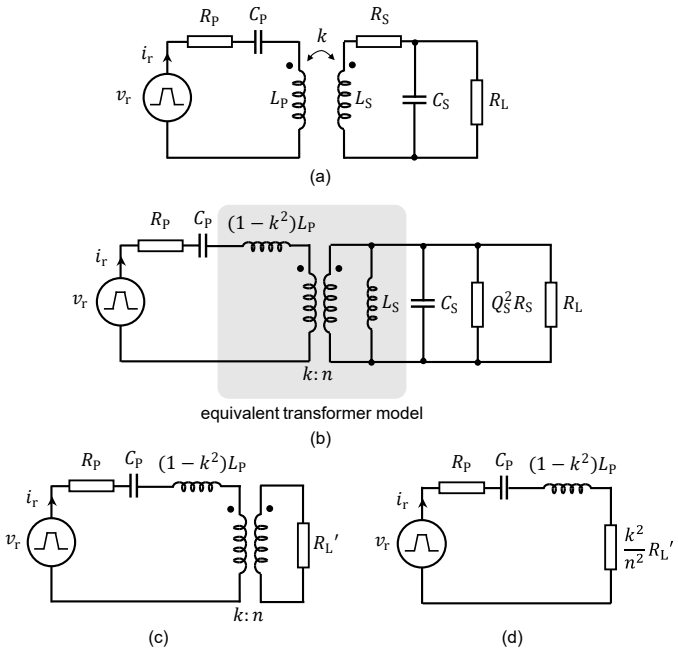

Fig. 3. (a) Series-parallel compensated resonant load, (b) simplified equivalent transformer model representation, (c) secondary side resonant components cancelled out and (d) equivalent simplified series resonant load.

Fig. 3(b) shows the transformer windings replaced by an equivalent model with an ideal transformer shown as highlighted portion [18]. The turns ratio of the ideal transformer is defined by $k : n$, where n is the turns ratio defined by the winding inductances as (6),

$$n = \sqrt{\frac{L_{\mathrm{R}}}{L_{\mathrm{T}}}} \tag{6}$$

In Fig. 3(b), the secondary side ESR (R_{S}) is transformed to parallel equivalent component $Q_{\mathrm{R}}^2 R_{\mathrm{R}}$, where Q_{R} is unloaded quality factor of secondary side [19]. In Fig. 3(b) on the secondary side, C_{S} is tuned such that it cancels out with secondary inductance (L_{S}) at the converter switching frequency ($f_{\mathrm{SW}} = 1/2\pi\sqrt{L_{\mathrm{S}}C_{\mathrm{S}}}$). This leads to the simplified load structure shown in Fig. 3(c). Finally the equivalent load resistance ($R'_{\mathrm{L}} = Q_{\mathrm{S}}^2 R_{\mathrm{S}} // R_{\mathrm{L}}$) is also moved to the primary side with turn-ratio transformation. This leads to the final equivalent simplified series resonant load as shown in Fig. 3(d).

For the hardware development, the air-core transformer secondary winding (L_{S}) is designed with a value of 3.1 μH. And the secondary side compensating capacitance (C_{S}) is tuned at 179 pF. This gives the Class-PN switching frequency (f_{SW}) of 6.76 MHz. The primary side compensating capacitor (C_{P}) is chosen to be 79 pF such that the natural frequency it forms with the primary side inductance ($(1 - k^2)L_{\mathrm{P}}$) is lower than Class-PN switching frequency (f_{SW}). The values for k, and L_{P} are 0.5 and 10 μH respectively. Thus the overall load natural frequency (f_0) seen by the Class-PN resonant converter is 6.5 MHz. Therefore the necessary condition for soft-switching operation of the semiconductor devices in Class-PN is maintained, i.e., $f_{\mathrm{SW}} > f_0$. Fig. 4 shows the hardware setup containing Class-PN resonant converter connected to series-parallel compensated resonant load. The load hardware development as well as the simplification steps in Fig. 3 are presented in detail in [20].

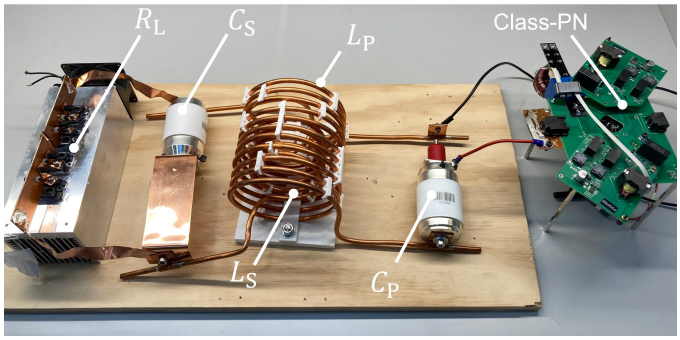

Fig. 4. Experimental setup containing Class-PN resonant converter connected to series-parallel resonant load.

Fig. 5 shows output waveform of Class-PN at four different operating conditions. The input DC link voltage (V_{DC}) is increased from 180 to 300 V, while the converter switching (f_{SW}) is kept constant at 6.76 MHz. The load utilized under all conditions is the same that is discussed previously. There are three signals in each waveform. The Class-PN output voltage (v_{r}) is measured by a high voltage, high frequency passive probe PPE2kV with a bandwidth of 400 MHz, whereas for Class-PN output current (i_{r}) measurement, a 50 MHz bandwidth current probe CP030 is used [21]. Along with Class-PN output current, its input DC current (I_{DC}) is also plotted. CP030 is also used for I_{DC} measurement. As indicated in Fig. 5, the measured phase angle (ψ_{meas}) is relatively constant for the four operating conditions as the load and the converter operating frequency (f_{SW}) are fixed. For the four operating conditions the phase angle has variation of only 0.5°, varying between 60.5° to 61°. Also indicated in the figure, are peak Class-PN output current (I_{SM}) as well as input DC current (I_{DC}) values for each of the operation conditions. The three measured quantities, ψ_{meas}, I_{SM} ,and I_{DC} are summarized in Table I. The Table also contains the calculated phase angle (ψ_{calc}) based on the (5). However it can be seen that the ψ_{calc} is significantly lower than ψ_{meas}. This is due to the current probe CP030 limited bandwidth of 50 MHz. Next section presents the discussion on probe bandwidth limitation.

TABLE I
VALUES FOR DIFFERENT OPERATING CONDITIONS IN FIG. 5.

Parameters	**DC link Voltage (V_{DC})**			
	180 V	**240 V**	**270 V**	**300 V**
ψ_{meas}	61°	61°	60.5°	60.5°
I_{SM}	4.25 A	5.6 A	6 A	6.8 A
I_{DC}	1.83 A	2.42 A	2.51 A	2.8 A
ψ_{calc} (5)	47.4°	47.2°	48.8°	50°

IV. ADJUSTMENT FOR PROBE RISE TIME

In Table I, the phase angle measurement (ψ_{meas}) is based on experimental waveform of Class-PN output voltage and current. It is noticed that the impact of probe bandwidth on the measurement has not be considered. Specifically the current probe (CP030), that is used to measure the current waveforms has a limited bandwidth of only 50 MHz. Using the probe rise time delay (t_{rise}) as given in (7) [21], [22]. This leads to rise time delay of 7 ns for the 50 MHz bandwidth CP030.

$$t_{\mathrm{rise}} = \frac{0.35}{BW} \tag{7}$$

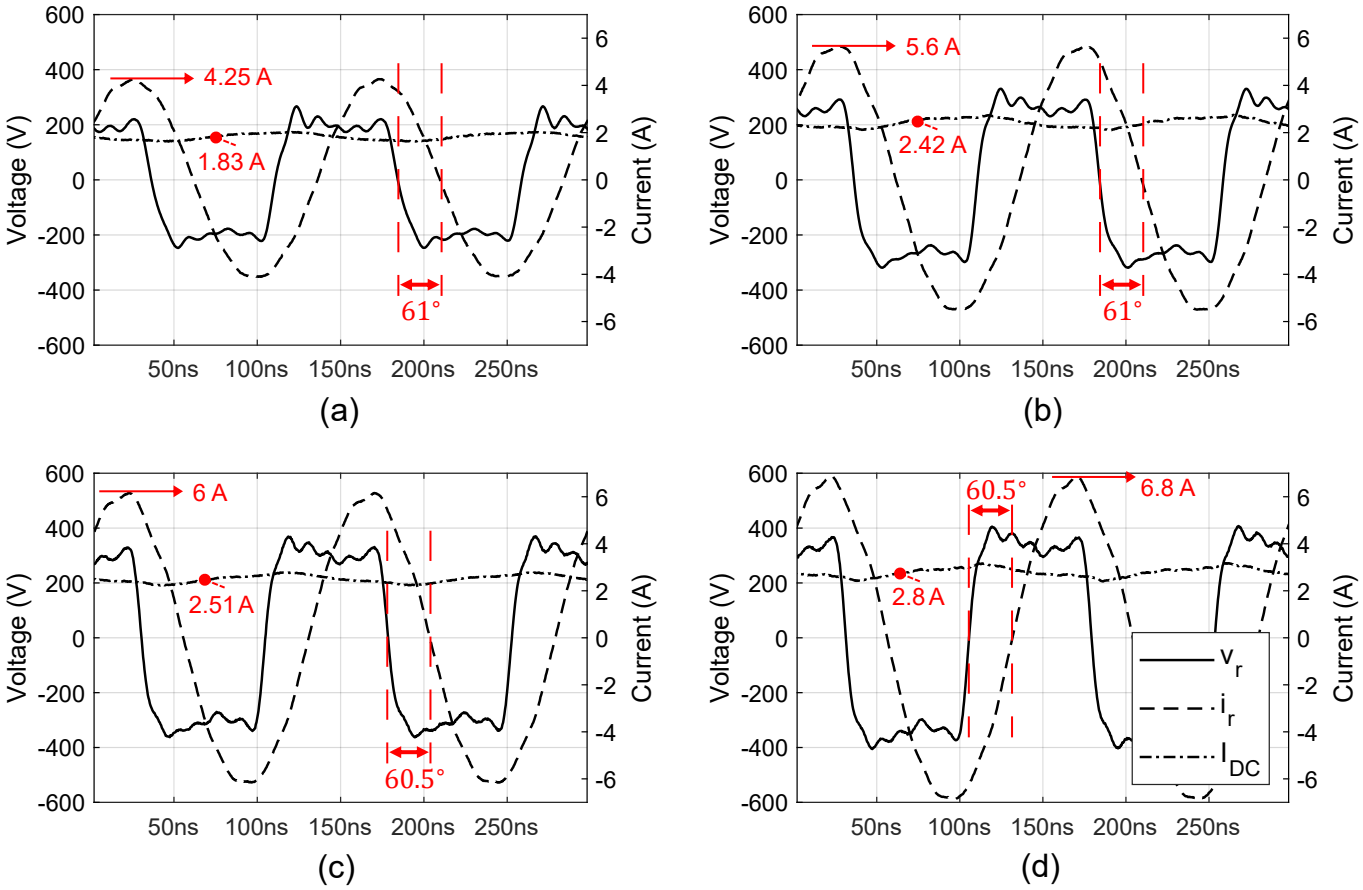

Fig. 5. Class-PN topology current and voltage waveforms at fixed f_{SW} of 6.76 MHz and different V_{DC} of (a) 180 V, (b) 240 V, (c) 270 V, and (d) 300 V.

The phase angle measurement is adjusted for the current probe rise time delay. The adjusted phase angle measurement ($\psi_{meas(adj)}$) is summarized for the four measurements in Table II.

TABLE II
FINAL VALUES FOR DIFFERENT OPERATING CONDITIONS.

Parameters	DC link Voltage (V_{DC})			
	180 V	**240 V**	**270 V**	**300 V**
ψ_{meas}	61°	61°	60.5°	60.5°
$\psi_{meas(adj)}$	44°	44°	43.4°	43.4°
ψ_{calc} (5)	47.4°	47.2°	48.8°	50°
error	3.4°	3.2°	5.4°	6.6°

In Table II the adjusted phase angle measurement ($\psi_{meas(adj)}$) and calculated phase angle (ψ_{calc}) have an error of only 3.2-6.6°.

V. Conclusion

The paper has presented a new method of using power handling capability to measure phase angle in Class-PN resonant topology. Experimental results have been shown to validate the proposed method. Based on the proposed method calculated phase angle has an error of 3.2-6.6° compared to experimentally measured waveforms when operating the resonant converter at 6.76 MHz. Therefore, novel controller circuit can be developed for ultra-high frequency resonant converters that does not require PLL or zero cross detection (ZCD).

References

[1] D. J. Perreault, J. Hu, J. M. Rivas, Y. Han, O. Leitermann, R. C. Pilawa-Podgurski, A. Sagneri, and C. R. Sullivan, "Opportunities and Challenges in Very High Frequency Power Conversion," in *2009 Twenty-Fourth Annual IEEE Applied Power Electronics Conference and Exposition*, 2009, pp. 1–14.

[2] O. Knecht, R. Bosshard, and J. W. Kolar, "High-Efficiency Transcutaneous Energy Transfer for Implantable Mechanical Heart Support Systems," *IEEE Transactions on Power Electronics*, vol. 30, no. 11, pp. 6221–6236, 2015.

[3] S. Li and C. C. Mi, "Wireless Power Transfer for Electric Vehicle Applications," *IEEE Journal of Emerging and Selected Topics in Power Electronics*, vol. 3, no. 1, pp. 4–17, 2015.

[4] O. Lucía, P. Maussion, E. J. Dede, and J. M. Burdío, "Induction Heating Technology and Its Applications: Past Developments, Current Technology, and Future Challenges," *IEEE Transactions on Industrial Electronics*, vol. 61, no. 5, pp. 2509–2520, 2014.

[5] J. M. Arteaga, S. Aldhaher, G. Kkelis, D. C. Yates, and P. D. Mitcheson, "Multi-MHz IPT Systems for Variable Coupling," *IEEE Transactions on Power Electronics*, vol. 33, no. 9, pp. 7744–7758, 2018.

[6] O. Lucia, J. M. Burdio, I. Millan, J. Acero, and D. Puyal, "Load-Adaptive Control Algorithm of Half-Bridge Series Resonant Inverter for Domestic Induction Heating," *IEEE Transactions on Industrial Electronics*, vol. 56, no. 8, pp. 3106–3116, 2009.

[7] S. Chudjuarjeen, A. Sangswang, and C. Koompai, "An Improved LLC Resonant Inverter for Induction-Heating Applications With Asymmetrical Control," *IEEE Transactions on Industrial Electronics*, vol. 58, no. 7, pp. 2915–2925, 2011.

[8] S. Dieckerhoff, M. Ruan, and R. De Doncker, "Design of an IGBT-based LCL-resonant inverter for high-frequency induction heating," in *Conference Record of the 1999 IEEE Industry Applications Conference. Thirty-Forth IAS Annual Meeting (Cat. No.99CH36370)*, vol. 3, 1999, pp. 2039–2045 vol.3.

[9] J. Ribas, J. Garcia, J. Cardesin, M. Dalla-Costa, A. J. Calleja, and E. L. Corominas, "High frequency electronic ballast for metal halide lamps based on a PLL controlled Class E resonant inverter," *PESC Record - IEEE Annual Power Electronics Specialists Conference*, vol. 2005, no. 1, pp. 1118–1123, 2005.

[10] J. C. Hernandez, M. C. Mira, L. P. Petersen, M. A. Andersen, and N. H. Petersen, "Zero Voltage Switching Control Method for MHz Boundary Conduction Mode Converters," *IEEE Transactions on Industrial Electronics*, vol. 67, no. 2, pp. 1544–1554, 2020.

[11] K. Wang, H. Zhu, J. Wu, X. Yang, and L. Wang, "Adaptive Driving Scheme for ZVS and Minimizing Circulating Current in MHz CRM Converters," *IEEE Transactions on Power Electronics*, vol. 36, no. 4, pp. 3633–3637, 2021.

[12] X. Wu, G. Hua, J. Zhang, and Z. Qian, "A New Current-Driven Synchronous Rectifier for Series–Parallel Resonant (LLC) DC–DC Converter," *IEEE Transactions on Industrial Electronics*, vol. 58, no. 1, pp. 289–297, 2011.

[13] W. Feng, F. C. Lee, P. Mattavelli, and D. Huang, "A Universal Adaptive Driving Scheme for Synchronous Rectification in LLC Resonant Converters," *IEEE Transactions on Power Electronics*, vol. 27, no. 8, pp. 3775–3781, 2012.

[14] M. Li, Z. Ouyang, M. A. E. Andersen, and B. Zhao, "Self-Driven Gate Driver for LLC Synchronous Rectification," *IEEE Transactions on Power Electronics*, vol. 36, no. 1, pp. 56–60, 2021.

[15] J.-D. Hsu, M. Ordonez, W. Eberle, M. Craciun, and C. Botting, "LLC Synchronous Rectification Using Resonant Capacitor Voltage," *IEEE Transactions on Power Electronics*, vol. 34, no. 11, pp. 10 970–10 987, 2019.

[16] F. Ahmad, A. B. Jørgensen, and S. Munk-Nielsen, "Four-switch Class-PN Power Amplifier for High Power Handling Capability in Wireless Power Transfer," in *2022 International Power Electronics Conference (IPEC-Himeji 2022- ECCE Asia)*, 2022, pp. 968–972.

[17] H. L. Krauss, W. Bostian, and F. H. Raab, "Solid State Radio Engineering," *New York: Wiley*, p. 472, 1980.

[18] K. V. Schuylenbergh and R. Puers, *Inductive Powering - Basic Theory and Application to Biomedical Systems*, 2009.

[19] R. R. Harrison, "Designing Efficient Inductive Power Links for Implantable Devices," *2007 IEEE International Symposium on Circuits and Systems*, pp. 2080–2083, 2007.

[20] F. Ahmad, A. B. Jørgensen, and S. Munk-Nielsen, "Modeling and Operation of Series-Parallel Resonant Load in Industrial RF Dielectric Heating Application," *IEEE Transactions on Industry Applications*, pp. 1–11, 2023.

[21] Teledyne Lecroy, "Current Probes," https://cdn.teledynelecroy.com/files/pdf/current-probes-datasheet.pdf, 2022, [Online; accessed June 2022].

[22] GaN Systems, "Measurement Techniques for High-Speed GaN E-HEMTs," https://gansystems.com/wp-content/uploads/2018/08/GN003-Measurement-Techniques-for-High-Speed-GaN-E-HEMTs_20180816.pdf, 2018, [Online; accessed March 2023].